Materials Science & Engineering C 116 (2020) 111277

Contents lists available at ScienceDirect

Materials Science & Engineering C

journal homepage: www.elsevier.com/locate/msec

Hybrid polymeric nanoparticles with high zoledronic acid payload and proton sponge-triggered rapid drug release for anticancer applications

Min-Cong Xiao[a], Ya-Hsuan Chou[a], Yu-Ning Hung[a], Shang-Hsiu Hu[b], Wen-Hsuan Chiang[a,*]

[a] Department of Chemical Engineering, National Chung Hsing University, Taichung 402, Taiwan
[b] Department of Biomedical Engineering and Environmental Sciences, National Tsing Hua University, Hsinchu 300, Taiwan

ARTICLE INFO

Keywords:
Zoledronic acid
Ionic complexes
Proton sponge-triggered drug release
Cancer therapy
Hybrid nanoparticles

ABSTRACT

Zoledronic acid (ZA), a third-generation nitrogen-heterocycle-containing bisphosphonate, has been frequently used as an anti-resorptive agent to treat cancer-involved hypercalcemia and painful bone metastases. In order to expand the clinical applications of ZA toward the extraskeletal tumor treatment, it is essential to develop the functionalized nanocarriers capable of carrying high ZA payload and achieving intracellular triggered ZA release. In this end, the ZA-encapsulated hybrid polymeric nanoparticles were fabricated in this work by *co*-association of the amphiphilic diblock copolymer poly(lactic-*co*-glycolic acid)-b-poly(ethylene glycol) (PLGA-b-PEG), tocopheryl polyethylene glycol succinate (TPGS) segments and ionic complexes composed of ZA molecules and branched poly(ethylenimine) (PEI) segments. Notably, the ionic pairings of PEI segments with ZA molecules not only assisted encapsulation of ZA into the PLGA-rich core of hybrid nanoparticles but also reduced adhesion of ZA on the surfaces of hydrophobic cores, thus largely increasing ZA loading capacity. The dynamic light scattering (DLS) and transmission electron microscopy (TEM) characterization revealed that the ZA/PEI-loaded nanoparticles had a well-dispersed spherical shape. Moreover, compared to short $PEI_{1.8k}$ (1.8 kDa) segments, the longer PEI_{10k} (10 kDa) segments formed more robust complexes with ZA molecules, thus prominently promoting ZA loading content of hybrid nanoparticles and their colloidal stability. Interestingly, with the suspension pH being reduced from 7.4 to 5.0, the considerable disruption of ZA/PEI ionic complexes owing to the acid-activated protonation of ZA molecules and the developed proton sponge-like effect inside the nanoparticle matrix upon the protonated PEI segments facilitated the rapid release of ZA molecules from drug-loaded hybrid nanoparticles. The results of in vitro cellular uptake and cytotoxicity studies showed that the ZA/PEI-loaded hybrid nanoparticles were internalized by MCF-7 cells upon energy-dependent endocytosis and displayed a superior cytotoxic effect to free ZA. This work demonstrates that the unique ZA/PEI-loaded hybrid polymeric nanoparticles display great promise for anticancer applications.

1. Introduction

Zoledronic acid (ZA), a third-generation nitrogen-heterocycle-containing bisphosphonate, has been extensively utilized as an anti-resorptive agent to treat osteoporosis and cancer bone metastasis [1–7]. Several clinical trials have reported that ZA can not only suppress skeletal tumor growth but also relieve cancer-involved bone diseases such as bone fracture and pain [1–7]. Moreover, through the inhibition of farnesyl diphosphate synthase (FPPS), a key enzyme of the mevalonate pathway, ZA can reduce cell migration, elicit apoptosis of cancer cells and suppress tumor growth in vitro in different types of cancer including breast and prostate cancer [8,9]. Furthermore, it was mentioned that ZA exhibited selective toxicity to tumor-associated macrophages (TAMs), thus showing promising potential for cancer immunotherapy [10–12]. Based on these studies, an antitumor potency of ZA has been demonstrated, however, the clinical translation of ZA as a cytotoxic agent to treat the extra-skeletal tumor are largely restricted due to its rapid elimination from plasma upon intravenous (i.v.) injection (blood circulation half-life of ca. 105 min) and massive adsorption by the bone tissue (ca. 55% of i.v.-administrated ZA) that considerably diminish the accumulation of ZA within the extra-skeletal tumor [12–16].

In order to enable the use of ZA on the treatment of extra-skeletal tumors, taking advantage of unique enhanced permeability and retention (EPR) effect of solid tumors, various nanoparticles such as liposomes [17,18], polymeric nanoassemblies [16,19], iron oxide nanoparticles [20], mesoporous silica nanocarriers (MSNs) [7,21] and nanoscaled metal-organic frameworks (nMOFs) [1,2,22] have been

* Corresponding author.
E-mail address: whchiang@dragon.nchu.edu.tw (W.-H. Chiang).

https://doi.org/10.1016/j.msec.2020.111277
Received 29 March 2020; Received in revised form 27 June 2020; Accepted 5 July 2020
Available online 07 July 2020
0928-4931/

developed as carriers of ZA. Among them, the ZA-loaded liposomes improved pharmacokinetics and biodistribution of ZA molecules to some extent, but did not show satisfied antitumor outcome owing to their relatively low drug loading (below 10%) [18]. To achieving high ZA loading, Wang and co-workers developed the folate-conjugated nMOF formulations of ZA composed of a hybrid dioleoylphosphatydic acid-coated calcium/ZA core and a poly(ethylene glycol) (PEG) surface by the water-in-oil micro-emulsion procedure [1]. The folate-conjugated calcium/ZA-based MOFs with a ZA loading content of 50.6 wt% not only possessed stable colloidal dispersion under physiological conditions but also realized intracellular release of ZA within the mid-endosomes. By the inhibition of tumor neovasculature and cancer cell proliferation, the calcium/ZA-based MOFs appreciably augmented antitumor capacity of ZA by 80–85% in vivo. Furthermore, the calcium/ZA nanocomplexes-encapsulated poly(lactic-*co*-glycolic acid) (PLGA) nanoparticles covered with octadecanoic acid-hydrazone-PEG (2000) segments were created by Cui's group [16]. The resultant ZA-containing nanoparticles effectively retarded premature ZA liberation in a simulated physiological environment and promoted cytotoxicity to both murine cancer cells and macrophages. The findings of in vivo study showed that the ZA-loaded PLGA-based nanoparticles not only increased deposition of ZA in orthotopically transplanted mammary tumors of mice but also considerably decreased the distribution of ZA in bones, thus exhibiting superior antitumor potency to the equivalent dose of free ZA. On the other hand, Rosenholm et al. have designed the poly(ethylenimine) (PEI)-modified MSNs to laden ZA and regulated ZA release rate by a tethered lipid bilayer acting as the “gate-keeper” [7]. Notably, the ZA-loaded nanocarriers after i.v.-injection remarkably reduced nonspecific accumulation of ZA within bone and inhibited tumor growth in breast tumor-bearing mice. In spite of the evident progress in targeted therapy of ZA to extra-skeletal tumors, it is a pity that the process of fabricating the aforementioned ZA-loaded nanoparticles involves the use of complicate materials, numerous organic solvents and multiple-step procedures, thus being not beneficial to large-scaled production and clinic translation.

To address the above issues, we herein report the fabrication of ZA/PEI-encapsulated hybrid polymeric nanoparticles by a simple single-step nanoprecipitation method. In this work, the amphiphilic diblock copolymer PLGA-b-PEG was utilized as the major component of ZA-loaded polymeric nanoparticles due to its excellent biodegradability and biocompatibility [23,24]. Furthermore, the D-α-tocopheryl polyethylene glycol succinate (TPGS) was employed to combine with the PLGA-b-PEG-based nanoparticles because of its amphiphilic nature and overcoming multiple drug resistance as the inhibitor of P-glycoprotein [25,26]. As shown in several studies [25–27], TPGS has been extensively utilized as a stabilizer, permeation enhancer, absorption enhancer, emulsifier, wetting agent and spreading agent while fabricating drug delivery systems. By the incorporation of ZA/PEI ionic complexes into the polymeric nanoparticles assembled by the amphiphilic PLGA-b-PEG and TPGS segments, the ZA loading efficiency was considerably promoted. Moreover, the structural characteristics of ZA/PEI-encapsulated nanoparticles were studied by variable angle dynamic light scattering (DLS), transmission electron microscopy (TEM), proton nuclear magnetic resonance (^{1}H NMR) and zeta potential measurements. The effects of molar ratio of amine and phosphonate groups from PEI and ZA, and of chain length of PEI segments on the physiochemical properties of ZA/PEI-encapsulated nanoparticles were further explored. Furthermore, in addition to the in vitro ZA release profile, the in vitro cellular uptake of ZA/PEI-encapsulated nanoparticles by MCF-7 cells and their in vitro cytotoxicity were also evaluated.

2. Experimental section

2.1. Materials

ZA was purchased from Tokyo Chemical Industry, CO., LTD (Japan). PLGA(50/50)-b-PEG$_{5k}$ (I.V. 0.21 dL/g) and PLGA(75/25)-b-PEG$_{5k}$ (I.V. 0.21 dL/g) were acquired from Green Square (Taiwan). Branched PEI$_{10k}$ (M.W. = 10 kDa) and PEI$_{1.8k}$ (1.8 kDa) were obtained from Alfa Aesar (USA). Dulbecco's modified Eagle medium (DMEM), Hoechst 33342, and fetal bovine serum (FBS) were purchased from Invitrogen (USA). TPGS, D_2O used in ^{1}H NMR measurements and 3-(4,5-Dimethylthiazol-2-yl)-2,5-diphenyltetrazolium bromide (MTT) were obtained from Sigma-Aldrich (USA). Deionized water was produced from Milli-Q Synthesis (18 MΩ, Millipore). All other chemicals were reagent grade and used as received. MCF-7 cells (human breast cancer cell line) and TRAMP-C1 (mouse prostate cancer cell line) were obtained from Food Industry Research and Development Institute (Hsinchu City, Taiwan).

2.2. Preparation of hybrid polymeric nanoparticles

Various hybrid polymeric nanoparticles loaded with either ZA alone or ZA/PEI ionic complexes were attained by one-step nanoprecipitation manner. The TPGS/PLGA(50/50)-b-PEG$_{5k}$ nanoparticles (referred hereinafter as TP1Ns) laden with ZA/PEI$_{10k}$ complexes were prepared as follows. First, ZA (3.2 mg) and branched PEI$_{10k}$ (4.6 mg) were dissolved in tris buffer of pH 8.5 and 6.0 (0.8 mL), respectively. The ZA solution was then added into PEI solution and stirred at 1000 rpm for 30 min to obtain the ZA/PEI mixtures. The ratio of the number of amine from PEI to the number of phosphonates from ZA (N/P ratio) was fixed at 4.5. TPGS (2.0 mg) in pH 7.4 tris buffer (0.1 mL) was added dropwise to the ZA/PEI mixtures under stirring at 1200 rpm. Subsequently, PLGA(50/50)-b-PEG$_{5k}$ (8.0 mg) dissolved in DMSO (0.3 mL) was added dropwise to the ZA/PEI/TPGS-containing aqueous solution (1.7 mL) under stirring. The mixed solution was gently stirred at 25 °C for 30 min, followed by an equilibration period of 1 h. The ZA/PEI-loaded TP1N suspension was dialyzed (Cellu Sep MWCO 12,000–14,000) against pH 7.4 phosphate buffer (10 mM) at room temperature to eliminate DMSO and unloaded ZA. For comparison, the pristine TP1Ns, ZA-loaded TP1Ns, ZA/PEI$_{10k}$-encapsulated TP1Ns (1.5) with an N/P ratio of 1.5 and ZA/PEI$_{1.8k}$-encapsulated TP1Ns (4.5) with an N/P ratio of 4.5 were also prepared in a similar manner. Furthermore, the TPGS/PLGA(75/25)-b-PEG$_{5k}$ nanoparticles (denoted hereinafter as TP2Ns) containing ZA/PEI$_{10k}$ ionic complexes with an N/P ratio of 4.5 were obtained by the same way.

2.3. Characterization of ZA/PEI$_{10k}$ ionic complexes and various hybrid polymeric nanoparticles

The zeta potential of free ZA, branched PEI$_{10k}$, ZA/PEI$_{10k}$ ionic complexes with N/P ratios of 1.5 and 4.5, and hybrid nanoparticles loaded with either ZA/PEI complexes or ZA alone in aqueous solution was measured by DLS using a ZetaSizer Nano Series instrument (Malvern Instruments, U.K.). In addition, the ^{1}H NMR measurement of free ZA, branched PEI$_{10k}$, ZA/PEI$_{10k}$ mixtures and ZA/PEI$_{10k}$-loaded TP1Ns (4.5) in D_2O, and of PLGA(50/50)-b-PEG and TPGS in $CDCl_3$ was conducted at 20 °C on a Agilent DD2 NMR spectrometer at 600 MHz. The particle size and size distribution (polydispersity index, PDI) of drug-free TP1Ns and the hybrid nanoparticles loaded with either ZA/PEI complexes or ZA alone in pH 7.4 phosphate-buffered saline (PBS) were determined by a Brookhaven BI-200SM goniometer equipped with a BI-9000 AT digital correlator using a solid-state laser (35 mW, λ = 637 nm) detected at a scattering angle of 90°. The data shown herein represent an average of at least triplicate measurements. Moreover, the angular dependence of the autocorrelation functions of various hybrid polymeric nanoparticles was assessed with the above apparatus. Correlation functions were attained by the cumulant method at different angles. The morphology of pristine and cargo-loaded hybrid nanoparticles was examined by TEM (JEOL JEM-1400 CXII microscope). TEM samples were prepared by placing some drops of the nanoparticle dispersion on a 300-mesh carbon-covered copper grid and

Table 1
Physiochemical properties, drug loading efficiency and content of ZA-containing hybrid nanoparticles.

Sample	D_h (nm)	PDI	[a]ZP (mV)	LE (%)	LC (wt%)
Pristine TP1Ns	115.6 ± 5.9	0.16 ± 0.03	−9.3 ± 0.9	–	–
ZA-loaded TP1Ns	201.1 ± 4.3	0.16 ± 0.03	−15.6 ± 0.7	23.3 ± 3.2	4.9 ± 0.6
ZA/PEI_{10k}-loaded TP1Ns (1.5)	139.9 ± 2.5	0.14 ± 0.05	3.0 ± 0.9	46.5 ± 1.4	10.6 ± 0.6
ZA/PEI_{10k}-loaded TP1Ns (4.5)	123.0 ± 1.8	0.13 ± 0.04	5.4 ± 1.3	90.1 ± 3.2	16.5 ± 0.5
ZA/$PEI_{1.8k}$-loaded TP1Ns (4.5)	149.2 ± 6.6	0.20 ± 0.05	−2.1 ± 0.9	38.0 ± 1.7	7.5 ± 0.2
ZA/PEI_{10k}-loaded TP2Ns (4.5)	130.4 ± 4.0	0.20 ± 0.03	0.43 ± 0.4	75.3 ± 2.9	14.2 ± 0.5

[a] ZP: zeta potential.

then negatively stained with uranyl acetate solution (2.0 wt%) for 20 s. The samples were dried at 25 °C for 2 days prior to TEM observation.

2.4. ZA encapsulation efficiency

In order to quantitatively determine ZA loading content, a small portion of ZA-containing nanoparticle suspension was lyophilized and then dispersed in DMSO to destroy the colloidal structure and enable ZA precipitation. The ZA precipitate was collected by centrifugal separation, followed by lyophilization. After freeze-drying, the ZA pellets were dissolved in deionized water. The absorbance of ZA at 210 nm was measured by UV/Vis spectrophotometer (U2900, Hitachi, Japan). The ZA calibration curve employed for drug loading characterization was revealed in Fig. S1. The loading efficiency (LE) and loading content (LC) of ZA were calculated as following formulas:

$$\text{LE (\%)} = (\text{weight of ZA loaded}/\text{weight of ZA in feed}) \times 100\%.$$

$$\text{LC (\%)} = (\text{weight of ZA loaded}/\text{total weight of ZA-containing hybrid nanoparticles}) \times 100\%.$$

2.5. In vitro ZA release

The in vitro ZA release of ZA/PEI_{10k}-encapsulated hybrid nanoparticles was executed by the dialysis method. The ICG/PEI-loaded nanoparticle suspension (1.0 mL) was placed within a dialysis tube (Cellu Sep MWCO 12,000–14,000), followed by dialysis against PBS (pH 7.4) and acetate buffer (pH 5.0) (ionic strength 0.15 M, 20 mL), respectively, at 37 °C. At the prescribed time intervals, 1.0 mL of dialysate (pH 5.0 or 7.4) was taken for analysis and replaced with an equivalent volume of fresh medium. ThermoFisher high-performance liquid chromatography (HPLC) with a reversed-phase C18 column (4.6 × 250 mm and 5 μm, Sigma-Aldrich (USA)) was utilized to determine the ZA concentration. The mobile phase was consisting of aqueous orthophosphoric acid solution (pH 6.0) and acetonitrile (88:12, v/v) with a gradient elution pumped at a flow rate of 1.0 mL/min, and the temperature of column was kept at 27 °C. The absorbance of ZA at 215 nm was determined. The data presented herein represent an average of triplicate measurements.

2.6. In vitro cellular uptake

Due to the lack of fluorescence property of ZA molecules, DiO, as a hydrophobic fluorescent dye, was encapsulated into ZA/PEI_{10k}-loaded TP2Ns for evaluating the cellular uptake using fluorescence imaging. MCF-7 cells (2×10^5 cells/well) were seeded in 6-well plate containing 22 mm round glass coverslips and cultured overnight. The cells were then incubated with DiO-labeled ZA/PEI_{10k}-loaded TP2Ns at 37 and 4 °C, respectively, for 1 h. Upon washing twice with PBS and fixing with 4% formaldehyde, the cells were stained with Hoechst 33342 for 5 min, and the slides were rinsed three times with PBS. Coverslips were placed onto the glass microscope slides, and the cellular uptake of DiO-labeled nanoparticles was visualized at the excitation wavelengths of 405 and 488 nm for Hoechst and DiO, respectively, by a confocal laser scanning microscope (CLSM) (Olympus, FluoView FV3000, Japan).

2.7. In vitro cytotoxicity study

MCF-7 cells were seeded in a 96-well plate at a density of 1×10^4 cells/well in DMEM (100 μL) containing 10% FBS and 1% penicillin, and incubated at 37 °C for 24 h. The medium was then replaced with 100 μL of fresh medium containing either free ZA or ZA/PEI_{10k}-loaded TP2Ns (4.5) at varying ZA concentrations or ZA-free TP2Ns, and cells were incubated at 37 °C for 48 h. Thereafter, 100 μL MTT (5.0 mg/mL) was added into each well, followed by incubation at 37 °C for 3 h. After discarding the culture medium, DMSO was added to dissolve the precipitate and the absorbance of the resulting solution at 570 nm was measured using a BioTek 800TS microplate reader.

3. Results and discussion

3.1. Preparation and characterization of ZA/PEI-encapsulated hybrid polymeric nanoparticles

To facilitate the use of ZA to treat extraskeletal tumors by boosting its concentration within tumor sites, it is requisite to reduce renal clearance and binding of ZA to bones following i.v. administration of this drug. In this end, the functionalized nanocarriers should be equipped with the capability of carrying high ZA payload and preventing ZA premature leakage during the blood circulation. In early stage of this study, through co-assembly of amphiphilic PLGA(50/50)-b-PEG_{5k} and TPGS segments in pH 7.4 aqueous solutions containing ZA molecules using the one-step nanoprecipitation procedure, the ZA-loaded TP1Ns were attained. Unfortunately, the ZA-loaded TP1Ns showed a quite low drug loading efficiency (ca. 26.2%) (Table 1). This result indicates that most of the hydrophilic ZA molecules were not efficiently encapsulated into the hydrophobic PLGA-constituted cores of TP1Ns due to their negatively-charged bisphosphonate groups. Notably, the zeta potential of TP1Ns upon the ZA loading at pH 7.4 was significantly shifted from −9.3 to −15.6 mV, revealing that ZA molecules were mainly adsorbed on the surfaces of hybrid nanoparticles, thus increasing negative charges on colloidal surfaces. Considering the easy condensation of positive charge-rich PEI segments with different negative ion-containing biomolecules (DNA or proteins) through neutralization or complexation [28,29], we assumed that it was possible to promote encapsulation of anionic ZA into the solid core of TP1Ns by forming hydrophobic electrostatic complexes with the positively-charged PEI segments. In order to verify the achievability of our strategy, by addition of aqueous ZA solution (pH 8.0) into PEI_{10k}-containing tris buffer solution (pH 6.0), the ZA/PEI_{10k} mixtures were obtained and characterized. As shown in Fig. 1a, the zeta potential of ZA molecules after being combined with PEI_{10k} segments at an N/P ratio of 1.5 was considerably changed from −10.8 mV to +5.1 mV. A similar zeta potential conversion was also attained in ZA/PEI_{10k} mixtures with an N/P ratio of 4.5. These data clearly signify the formation of ZA/PEI_{10k} ionic complexes upon the electrostatic attraction of

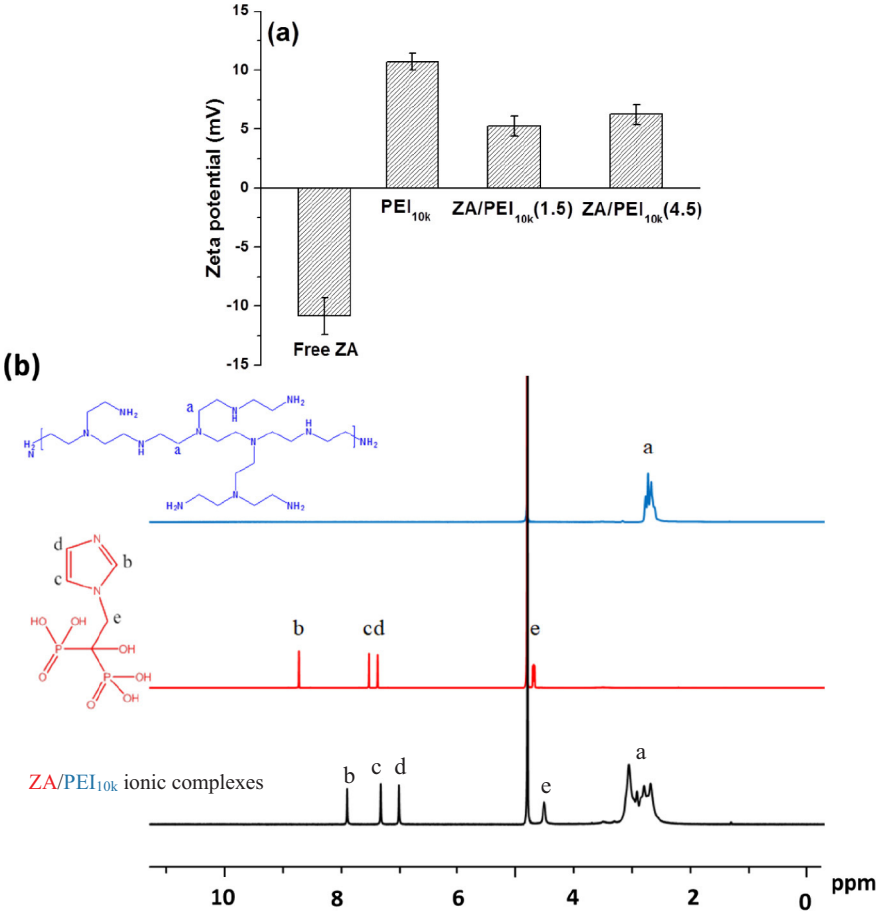

Fig. 1. (a) Zeta potential values of free ZA, PEI_{10k} and ZA/PEI_{10k} ionic complexes in aqueous solutions. (b) ^1H NMR spectra of PEI_{10k}, free ZA and ZA/PEI_{10k} ionic complexes in D_2O.

bisphosphonate and amine groups from ZA molecules and PEI_{10k} segments. On the other hand, the development of ionic pairings between ZA molecules and PEI_{10k} segments was further demonstrated by the ^1H NMR measurement. As presented in Fig. 1b, the characteristic proton signals of imidazole and methylene groups of free ZA in D_2O appeared at δ 7.4, 7.5, 8.8 and 4.7 ppm, respectively, while the corresponding proton signals of ZA from the ZA/PEI_{10k} mixtures became significantly up-field shifted. Such an up-field shift of proton signals could be attributed to the enhanced electron shielding effect on proton-nucleus of ZA molecules complexed with the PEI_{10k} segments. Moreover, in comparison with PEI segments alone, the ZA/PEI_{10k} mixtures showed the broader PEI proton signals, being indicative of a remarkable increase in the environmental heterogeneity of the coupled PEI segments. The findings of ^1H NMR and zeta potential characterization strongly confirm the generation of ZA/PEI_{10k} ionic complexes.

On the basis of the above observation, PEI_{10k} was employed for the preparation of the ZA/PEI_{10k}-loaded TP1Ns. As shown in Table 1, the drug loading efficiency of ZA/PEI_{10k}-loaded TP1Ns (N/P ratio = 1.5) determined to be ca 46.5% was higher than that (ca 23.3%) of the ZA-loaded TP1Ns. Notably, when the N/P ratio of ZA/PEI_{10k} complexes in feed was raised from 1.5 to 4.5, the drug loading efficiency of ZA/PEI_{10k}-loaded TP1Ns was largely increased from 46.5 to 90.1%. Different from the ZA-loaded TP1Ns with the significantly negative zeta potential value, the ZA/PEI_{10k}-loaded TP1Ns showed slightly positive zeta potential values (Table 1). These results suggest that the formation of more ZA/PEI_{10k} ionic complexes really assists the encapsulation of ZA into the hydrophobic core of TP1Ns instead of their surfaces. Although the drug loading content (16.5 wt%) of ZA/PEI_{10k}-loaded TP1Ns (4.5) is lower than that (50.6 wt%) of the folate-conjugated calcium/ZA-based MOFs developed by Wang's group [1], it is noteworthy to mention that, in comparison with the complicated processes adopted to prepare the calcium/ZA-based MOFs, the current strategy of fabricating ZA/PEI-loaded polymeric nanoparticles has several advantages including the one-step co-assembly procedure, unnecessary numerous organic solvents and surfactants, and low material cost.

On the other hand, compared with the ^1H NMR spectra of ZA/PEI_{10k} ionic complexes in D_2O, PLGA(50/50)-b-PEG_{5k} and TPGS segments in $CDCl_3$ (Figs. 1b, 2a and b), the significantly declined signal intensity of the methyl protons of PLGA and TPGS segments at δ 1.40 and 0.81 ppm, respectively, and the weak feature proton signals of ZA molecules and PEI segments at δ 7.0, 7.4, 8.0 and 2.5–3.2 ppm, respectively, were observed in the ^1H NMR spectrum of ZA/PEI_{10k}-loaded TP1Ns (4.5) in D_2O (Fig. 2c). This signifies that the PLGA segments of PLGA(50/50)-b-PEG_{5k}, vitamin E moieties of TPGS, and ZA/PEI_{10k} ionic complexes are involved extensively in the development of hydrophobic core of hybrid nanoparticles during co-association, rendering their corresponding protons undetectable by ^1H NMR. By contrast, the characteristic signals of ethylene protons at δ 3.75 ppm of PEG segments of PLGA(50/50)-b-PEG_{5k} and TPGS from ZA/PEI_{10k}-loaded TP1Ns remained appreciably detectable, suggesting that the hydrophilic PEG segments mostly resided at the surfaces of TP1Ns, thus extensively interacting with water molecules to maintain the outstanding segmental mobility. Based on the above findings, it can be conceivable that the resultant ZA/PEI_{10k}-loaded TP1Ns have a hydrophobic ZA/PEI_{10k} ionic complexes-containing PLGA-rich core covered by the highly hydrated PEG segments (Scheme 1).

Furthermore, the DLS data illustrated that the ZA/PEI_{10k}-loaded TP1Ns (4.5) and ZA-loaded TP1Ns had a monomodal size distribution

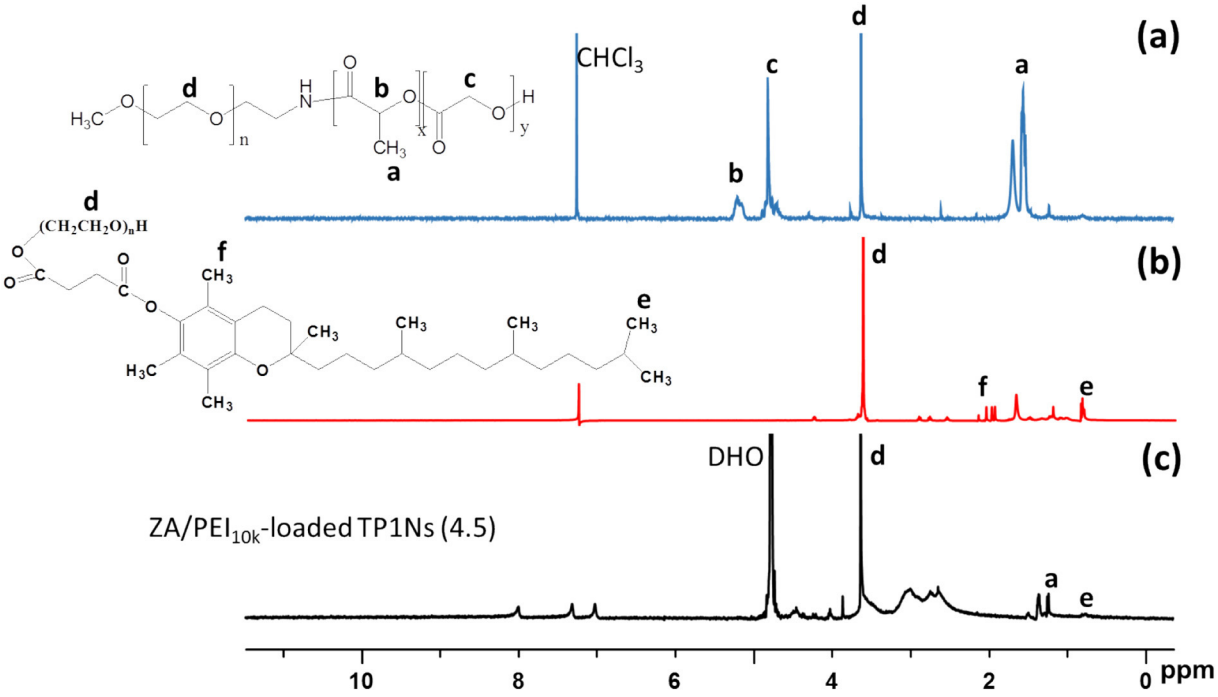

Fig. 2. ^{1}H NMR spectra of (a) PLGA(50/50)-b-PEG$_{5k}$ and (b) TPGS segments in $CDCl_3$, and (c) ZA/PEI$_{10k}$-loaded TP1Ns (4.5) in D_2O.

in PBS and the mean hydrodynamic diameter (ca. 123.0 nm) of the former was considerably smaller than that of the latter (ca. 201.1 nm) (Table 1 and Fig. 3a). The enlarged particle size of ZA-loaded TP1Ns may be ascribed that, in the absence of PEI segments, most of the anionic ZA molecules adhered on the surfaces of TP1Ns probably render the core more hydrated, thus increasing the aggregation number of PLGA-b-PEG and TPGS segments during co-association process to stabilize colloidal structure. Similar findings were also reported by Pauletti and colleagues [30]. In their study, the particle size of nanostructured lipid carriers (NLCs) containing bisphosphonate-bearing alendronate (AL)/PEI ionic complexes was appreciably smaller in comparison with that of NLCs loaded with AL alone. This was because, in the lack of PEI segments, the presence of the anionic bisphosphonate drug increased the volume fraction of aqueous phase encapsulated within the lipid matric, thus enlarging the particle size of AL-loaded NLCs. On the other hand, to gain an insight into the morphology of various ZA-containing nanoparticles in PBS, the variable angle DLS measurements were conducted. Notably, for the ZA/PEI$_{10k}$-loaded TP1Ns (4.5), a high linear relationship (R^2 = 0.99) between the relaxation frequency (Γ) and the square of the scattering vector (q^2) was obtained (Fig. 3b). This indicates that these nanoparticles in aqueous solution exhibited a spherical form [31–33]. By contrast, as presented in Fig. 3c, a low linear relationship (R^2 = 0.96) of Γ versus q^2 of ZA-loaded TP1Ns implies their morphology in a non-spherical particle shape. Corresponding to the angle-dependent DLS data, the TEM images (Fig. 3d and e) revealed the well dispersion of pristine TP1Ns and ZA/PEI$_{10k}$-loaded TP1Ns (4.5) as individual spherical colloidal particles, whereas the TEM images in Fig. 3f showed the non-spherical shape of ZA-loaded TP1Ns. Also, a remarkably larger particle size of ZA-loaded TP1Ns compared to that of ZA/PEI$_{10k}$-loaded TP1Ns (4.5) was observed in TEM images (Fig. S2). Herein it should be noted that the particle sizes of TP1Ns observed by TEM were somewhat smaller than those determined by DLS due to their conversion from dried state (TEM) to swollen stats (DLS) [34,35]. Moreover, the polydisperse size distribution of the pristine TP1Ns and ZA-containing TP1Ns observed in the TEM images could be ascribed to their different dehydration degree during the drying of TEM samples.

In this work, in order to investigate the effect of molecular weight of PEI segments on the drug loading efficiency of ZA/PEI-loaded TP1Ns and their colloidal stability in PBS, the short branched PEI$_{1.8k}$ segments instead of the long branched PEI$_{10k}$ segments were adopted to fabricate

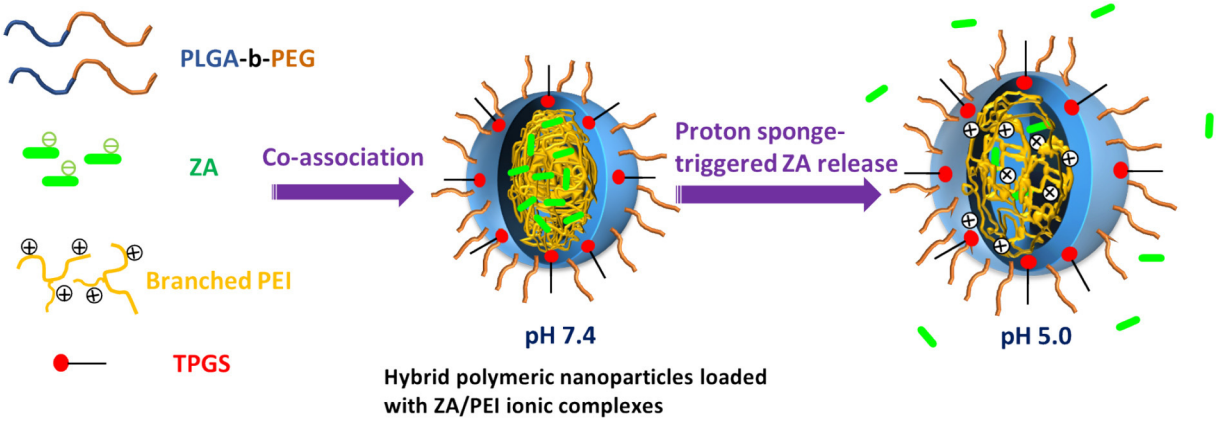

Scheme 1. Schematic illustration of development of ZA/PEI-loaded hybrid polymeric nanoparticles and their proton sponge-triggered ZA release.

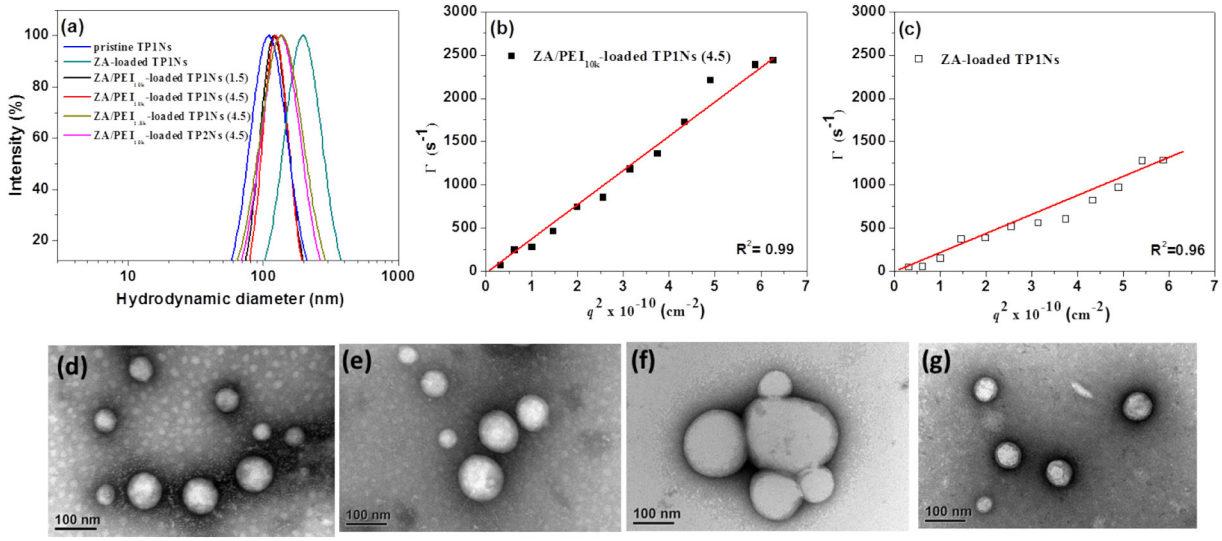

Fig. 3. (a) DLS size distribution profiles of polymeric nanoparticles in pH 7.4 PBS. Angle-dependent correlation of Γ versus q^2 of (b) ZA/PEI_{10k}-loaded TP1Ns (4.5) and (c) ZA-loaded TP1Ns in pH 7.4 PBS. TEM images of (d) pristine TP1Ns, (e) ZA/PEI_{10k}-loaded TP1Ns (4.5), (f) ZA-loaded TP1Ns and (g) ZA/PEI_{10k}-loaded TP2Ns (4.5).

the ZA/$PEI_{1.8k}$-encapsulated TP1Ns with an N/P ratio of 4.5. Notably, a much lower drug loading efficiency (ca. 38.0%) of ZA/$PEI_{1.8k}$-loaded TP1Ns in comparison with that (ca. 90.1%) of ZA/PEI_{10k}-loaded TP1Ns was obtained (Table 1). Several studies pointed out that the electrostatic assembly of long branched PEI segments with negatively charged species (e.g. siRNA and DNA) tended to form more compact ionic pairings [36,37]. Therefore, such a difference in ZA loading efficiency could be attributed to that the long branched PEI_{10k} segments were apt to form more dense and stable ionic complexes with negatively-charged ZA molecules, thus promoting amount of ZA embedded within hybrid core of the TP1Ns, while the incorporation of loose ZA/$PEI_{1.8k}$ complexes into the PLGA cores was not able to sufficiently prevent ZA leakage during the dialysis-involved purification, thus largely reducing the drug loading efficiency of ZA/$PEI_{1.8k}$-loaded TP1Ns.

3.2. Colloidal stability of ZA/PEI-containing hybrid polymeric nanoparticles

Because the colloidal stability of ZA-carrying nanoparticles in the aqueous solution play an important role in practical anticancer applications, the colloidal stability of ZA/PEI-loaded nanoparticles in PBS (I = 0.15 M) containing 10% FBS or not at 37 °C was evaluated by monitoring their size variation over time. As shown in Fig. 4a and b, no significant variation in particle size was observed within 24 h for ZA/PEI_{10k}-loaded TP1Ns in PBS, while a significantly enlarged particle size of ZA/$PEI_{1.8k}$-loaded TP1Ns after 12 h was attained. Obviously, the ZA/PEI_{10k}-loaded TP1Ns maintained stable colloidal structure in PBS, whereas the ZA/$PEI_{1.8k}$-loaded TP1Ns became somewhat swollen, probably because the loose ZA/$PEI_{1.8k}$ ionic complexes were partly destroyed by salt ions, thus facilitating water influx. On the other hand, when the ZA/PEI_{10k}-loaded TP1Ns were dispersed in PBS containing 10% FBS, their particle size was remarkably enlarged from 123 to 225 nm within 24 h (Fig. 4c), being indicative of the inter-particle aggregation. In view of the positive zeta potential value (ca. +5.4 mV) of ZA/PEI_{10k}-loaded TP1Ns (4.5) (Table 1), the non-specific adsorption of serum proteins to the positive-charged surfaces of ZA/PEI_{10k}-loaded TP1Ns probably further elicited the inter-particle aggregation. Similar results were also mentioned elsewhere [38,39]. In order to achieve effective tumor-targeted ZA delivery, the aggregation of the ZA/PEI-containing nanoparticles in FBS-containing environment should be significantly inhibited to avoid their rapid clearance by the mononuclear phagocyte system and prolong their blood circulation time. In this end, the PLGA(75/25)-b-PEG_{5k} instead of PLGA(50/50)-b-PEG_{5k} was used to prepare ZA/PEI_{10k}-loaded TP2Ns with an N/P ratio of 4.5. As shown in the results of DLS measurement and TEM observation (Table 1, Figs. 3a and g, and S2 and S3), the ZA/PEI_{10k}-loaded TP2Ns (4.5) exhibited comparable particle size and morphology to ZA/PEI_{10k}-loaded TP1Ns (4.5). Also, the ZA/PEI_{10k}-loaded TP2Ns (4.5) showed a satisfied ZA loading capacity (LE: 75.3% and LC: 14.2%). More importantly, in FBS-containing PBS at 37 °C, the ZA/PEI_{10k}-loaded TP2Ns maintained unvaried particle size for 24 h (Fig. 4d), illustrating their superior colloidal stability to that of the ZA/PEI_{10k}-loaded TP1Ns. This may be attributed to that the nearly neutral (zeta potential of ca. 0.43 mV) and PEG-rich surfaces of ZA/PEI_{10k}-loaded TP2Ns could hinder the adsorption of serum protein, thereby preventing inter-particle aggregation. Furthermore, it should be mentioned that the ZA/PEI_{10k}-encapsulated TP2Ns suffered from large-volume dilution with PBS still remained unchanged particle size (Fig. S4). In this regard, it was anticipated that the robust ZA/PEI_{10k}-loaded TP2Ns after intravenous administration could reserve structural integrity during blood circulation to avoid undesired inter-particle aggregation and premature particle dissociation.

3.3. In vitro release of ZA from ZA/PEI-encapsulated hybrid polymeric nanoparticles

To assess if undesired burst leakage of ZA from the developed ZA/PEI-loaded nanoparticles occurs at physiological pH (i.e. pH 7.4), the in vitro ZA release test was studied by dialysis method. As shown in Fig. 5, compared to quick diffusion of free ZA molecules across the dialysis tube in pH 7.4 PBS (over 95% within 2 h), only less than 20% of ZA was released from the ZA/PEI_{10k}-loaded TP2Ns (4.5) within 24 h under the same condition. Such a remarkably reduced burst release of ZA was also observed for ZA/PEI_{10k}-loaded TP1Ns (4.5) in PBS at pH 7.4 (Fig. S5). Under the mimetic physiological conditions, as compared to the other ZA-loaded nanoformulations (i.e. lipid-coated calcium/ZA nanoparticles with above 35% ZA release over 24 h [2] and the ZA-carrying hydroxyapatite nanoparticles with premature ZA outflow (over 60% ZA release within 60 min) [40]), the ZA/PEI_{10k}-loaded TP2Ns developed in this work potently inhibited ZA leakage by means of the dense PLGA-rich core acting as a barrier capable of stabilizing inner ZA/PEI ionic complexes. Interestingly, for ZA/PEI_{10k}-loaded TP2Ns at pH 5.0, more than 50% of ZA was rapidly released over a period of 1 h. Here, it should be noted that the acid-triggered rapid drug release of ZA/PEI_{10k}-

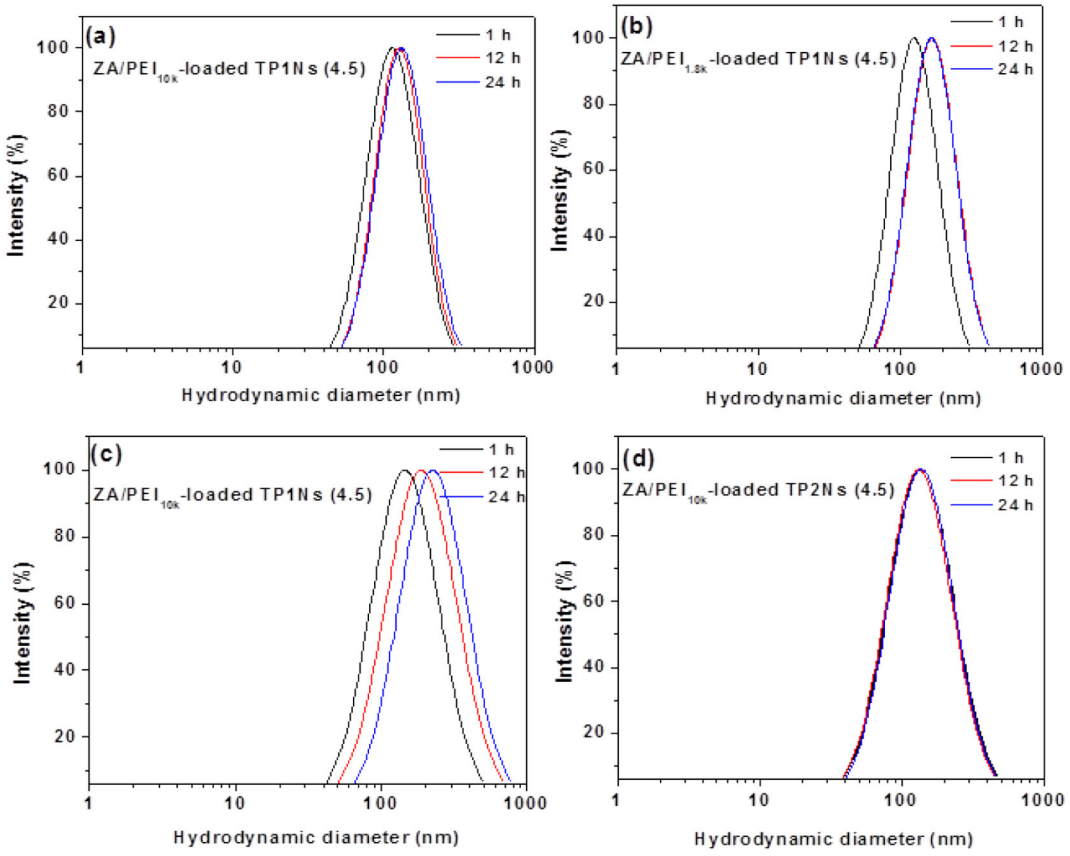

Fig. 4. DLS size distribution profiles of (a) ZA/PEI_{10k}-loaded TP1Ns (4.5) and (b) ZA/$PEI_{1.8k}$-loaded TP1Ns (4.5) dispersed in pH 7.4 PBS, (c) ZA/PEI_{10k}-loaded TP1Ns (4.5) and (d) TP2Ns (4.5) suspended in PBS containing 10% FBS at different time intervals.

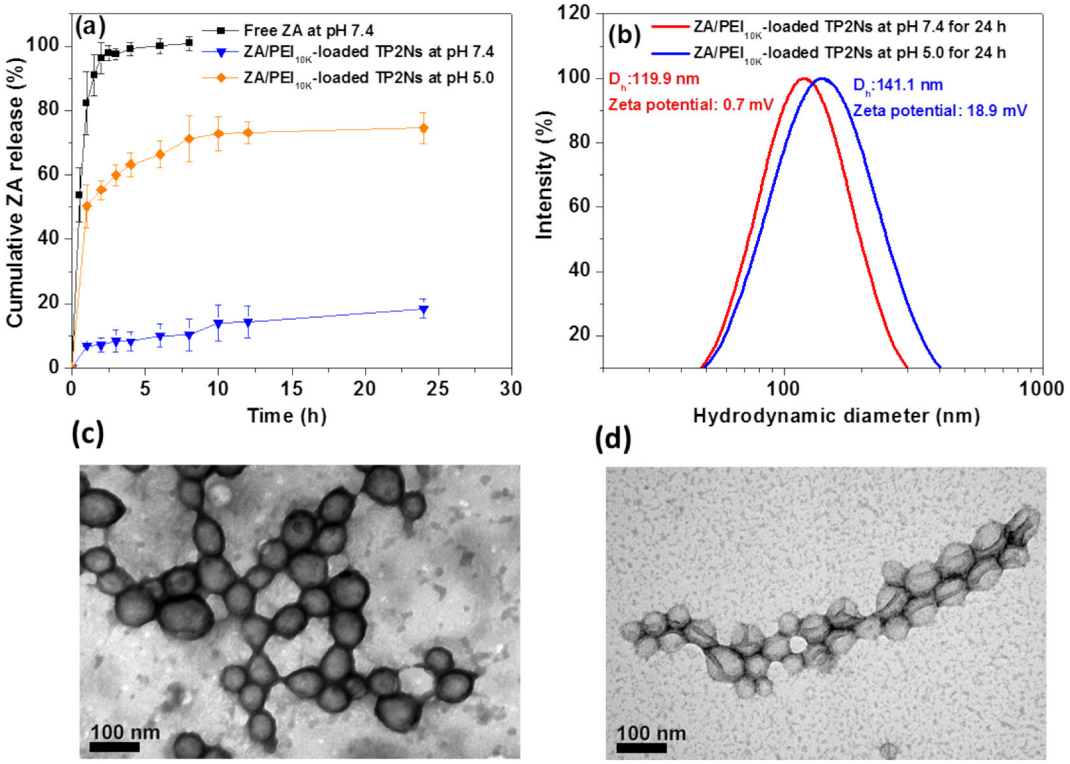

Fig. 5. (a) Cumulative ZA release profiles of ZA/PEI_{10k}-loaded TP2Ns (4.5) at pH 5.0 and 7.4 at 37 °C using the dialysis method. Diffusion of free ZA through the dialysis tube is included for comparison. (b) DLS size distribution profiles of ZA/PEI_{10k}-loaded TP2Ns after 24-h in vitro drug dissolution test of pH 7.4 and 5.0, respectively. TEM images of ZA/PEI_{10k}-loaded TP2Ns after 24-h in vitro drug dissolution test at pH 7.4 (c) and 5.0 (d), respectively.

loaded TP2Ns is significantly different from the sustained drug release of the traditional PLGA-based nanoformulations over a long period of time (from days to months) through diffusion of drug molecules and/or by hydrolytic erosion of the PLGA nanoparticles, or by a combination of both [41–43]. In order to understand the mechanism of acid-triggered rapid ZA liberation, the structural variation of ZA/PEI_{10k}-loaded TP2Ns after in vitro drug dissolution test at different pH was characterized by DLS and TEM measurements. As revealed in Fig. 5b, after 24-h in vitro drug dissolution test, in addition to the enlarged mean particle size of ZA/PEI_{10k}-loaded TP2Ns from 119.9 to 141.1 nm in response to pH change from 7.4 to 5.0, their zeta potential was also evidently shifted from 0.7 to 18.9 mV. These results indicate that the surface positive charges of ZA/PEI_{10k}-loaded TP2Ns were remarkably increased at pH 5.0 due to the acid-activated protonation of the amines of uncomplexed PEI segments of the hybrid nanoparticles. Such an enhanced protonation of inner PEI segments could enable the development of osmotic pressure inside the ZA/PEI_{10k}-loaded TP2Ns, thus promoting water influx to allow nanoparticles somewhat swollen. Furthermore, the TEM images in Fig. 5c and d showed that the ZA/PEI_{10k}-loaded TP2Ns suffering 24-h drug dissolution test at pH 7.4 still maintained the relatively intact colloidal structure, but turned into capsule-like architecture at pH 5.0. Similar TEM images of capsule-like polymeric nanoparticles were also presented in the literatures [44,45]. Such an acid-triggered morphology transformation of ZA/PEI_{10k}-loaded TP2Ns implies that their structure became quite loose and hydrated at pH 5.0 due to the increased protonation of PEI segments and then water inflow, thus being apt to deform during drying of TEM specimens.

Based on the above results, for ZA/PEI_{10k}-loaded TP2Ns, the mechanism of acid-triggered ZA rapid liberation was ascribed to following reasons. First, the well-known bulk erosion of PLGA-based core occurred as water diffusion into the matrix is faster than polymer erosion [46], thus largely destroying the inner ZA/PEI_{10k} ionic complexes upon the lowered electrostatic attraction driven by the acid-activated protonation of imidazole groups of ZA molecules (pKa_1 = 5.9 [1]). Meanwhile, due to the increased protonation of amine residues of PEI segments in acidic environment [47,48], the proton sponge-like effect of positively-charged PEI segments within the TP2Ns established osmotic pressure inside the nanoparticle matrix and allowed quick influx of water molecules, thus assisting the fast diffusion of water-soluble ZA molecules from partially degraded PLGA cores to the external aqueous phase (Scheme 1). Similarly, as mentioned by Jain et al., the presence of amine-rich chitosan in the PLGA nanoparticles facilitated the development of osmotic pressure within the nanoparticle, thus considerably accelerating the rate of erosion of the nanoparticles and drug payload release [46]. Considering the inherent pH difference between the blood/normal tissues (pH 7.4) and intracellular acidic endosomes and lysosomes (pH 6.0–4.5) [2,11,31], it is expected that the pH-dependent release of ZA from ZA/PEI_{10k}-loaded TP2Ns will likely be beneficial for minimum premature ZA leakage during blood circulation and maximum intracellular ZA delivery to promote extraskeletal tumor treatment.

3.4. Cellular uptake and in vitro cytotoxicity of ZA/PEI-loaded hybrid polymeric nanoparticles

Due to lack of fluorescence property of ZA molecules, a hydrophobic fluorescent dye, DiO, was encapsulated into the ZA/PEI_{10k}-loaded TP2Ns (4.5) for observing the cellular uptake of ZA/PEI_{10k}-loaded TP2Ns by MCF-7 cells using fluorescence imaging. As shown in the CLSM images (Fig. 6), visible DiO fluorescence signals were mainly found within the cytoplasm of MCF-7 cells incubated with DiO-labeled ZA/PEI_{10k}-carrying TP2Ns at 37 °C for 1 h. By contrast, no significant DiO fluorescence was observed from MCF-7 cells incubated with DiO-labeled ZA/PEI_{10k}-carrying TP2Ns at 4 °C for 1 h. The results illustrate that the cellular uptake of cargo-loaded TP2Ns could be realized via the energy-dependent endocytosis pathway. It is well known that most of nanoparticle-based drug delivery systems are internalized by cancer cells via endocytosis-mediated pathway [1,11,49–51]. Upon the cellular uptake of ZA/PEI_{10k}-loaded TP2Ns via endocytosis, it was expected that the intracellular ZA delivery could be achieved by the acid-triggered rapid ZA liberation of ZA/PEI_{10k}-loaded TP2Ns within acidic endosomes and lysosomes, thereby maximizing the anticancer efficacy.

The in vitro cytotoxicity of ZA/PEI_{10k}-loaded TP2Ns (4.5) against MCF-7 cells was further evaluated by MTT assay. As an essential control, high viability (over 90%) of MCF-7 cells treated with ZA-free TP2Ns in the concentration range 1.6–832 μg/mL for 48 h was attained (Fig. 7a), illustrating that the drug-free TP2Ns were nearly nontoxic to MCF-7 cells. By contrast, the viability of MCF-7 cells incubated with free ZA molecules and ZA/PEI_{10k}-loaded TP2Ns, respectively, was remarkably reduced with increased ZA concentration (Fig. 7b), proving the anticancer effect of ZA molecules. Notably, the drug doses required for 50% cellular growth inhibition (IC_{50}) of ZA/PEI_{10k}-loaded TP2Ns is ca. 37.5 μM lower than that (ca. 87.5 μM) of free ZA, revealing that the ZA/PEI_{10k}-loaded TP2Ns exhibit superior cytotoxic effect to free ZA species. Also, compared to free ZA, the ZA/PEI_{10k}-loaded TP2Ns showed the higher efficacy in inhibiting the proliferation of TRAMP-C1 cells (Fig. 7c). Such an enhanced anticancer capability of ZA/PEI_{10k}-loaded TP2Ns relative to free ZA molecules could be attributed to the following two reasons. First, compared to highly water-soluble and negatively-charged ZA molecules, the ZA/PEI_{10k}-loaded TP2Ns featuring a near-neutral and TPGS-containing surface were most likely internalized by cancer cells in a more efficient manner, leading to a higher intracellular ZA concentration. Some studies also reported that the encapsulation of bisphosphonates into nanoparticle-based delivery systems remarkably enhanced their antitumor efficacy by the improved cellular uptake [16,52]. Second, the acid-activated rapid ZA release of ZA/PEI_{10k}-loaded TP2Ns within acidic organelles could maximum the anticancer effect of ZA.

4. Conclusions

In this work, the ZA/PEI-encapsulated hybrid polymeric nanoparticles were developed by co-association of the amphiphilic PLGA-b-PEG, TPGS segments and ionic complexes composed of ZA molecules and branched PEI segments. The encapsulation of ZA/PEI_{10k} ionic complexes into the PLGA-rich core of hybrid nanoparticles largely increased ZA loading. The resultant ZA/PEI_{10k}-loaded TP2Ns were characterized to have a well-dispersed spherical shape and showed several excellent properties, including (1) superior colloidal stability, (2) effectively reduced ZA leakage at physiological pH, (3) acid-triggered rapid ZA release, and (4) promoted intracellular ZA delivery and anticancer effect. This work demonstrates that the unique ZA/PEI-loaded hybrid polymeric nanoparticles display great promise for anticancer applications.

CRediT authorship contribution statement

Min-Cong Xiao:Conceptualization, Investigation, Resources, Writing - original draft.**Ya-Hsuan Chou**:Investigation, Validation, Methodology.**Yu-Ning Hung**:Investigation, Resources.**Shang-Hsiu Hu**:Writing - review & editing.**Wen-Hsuan Chiang**:Conceptualization, Writing - review & editing, Supervision, Project administration, Funding acquisition.

Declaration of competing interest

The authors declare that they have no known competing financial interests or personal relationships that could have appeared to influence the work reported in this paper.

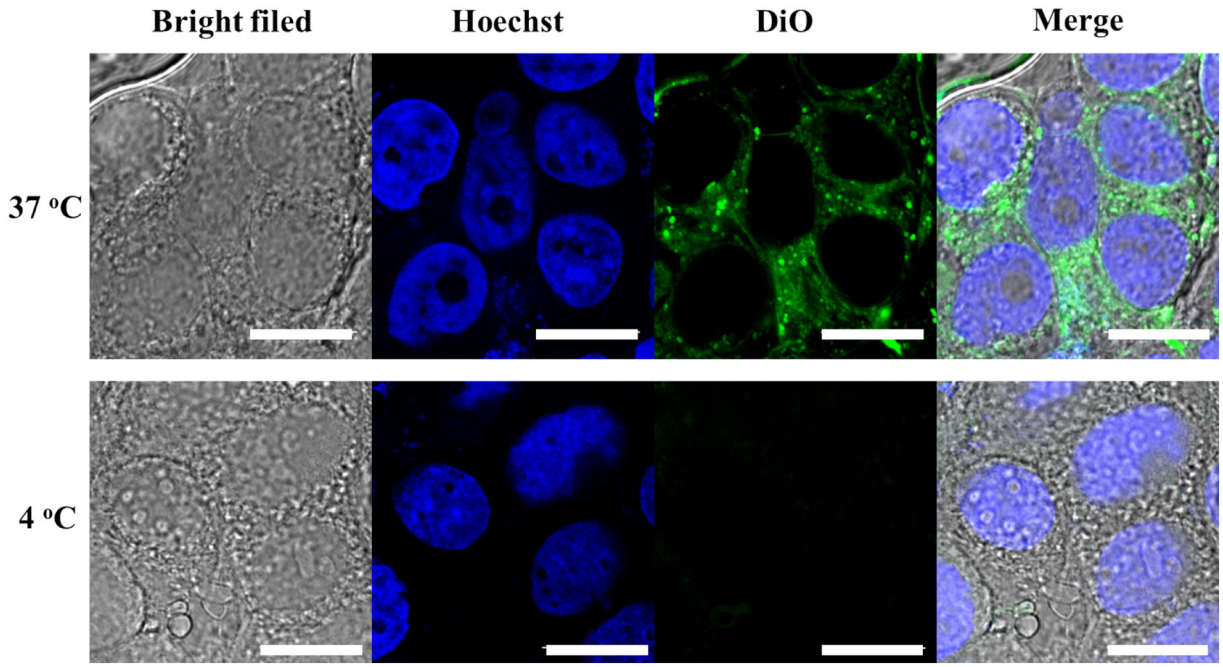

Fig. 6. CLSM images of MCF-7 cells incubated with DiO-labeled ZA/PEI_{10k}-loaded TP2Ns (4.5) at 37 and 4 °C, respectively, for 1 h. Cell nuclei were stained with Hoechst 33342. Scale bars are 15 μm.

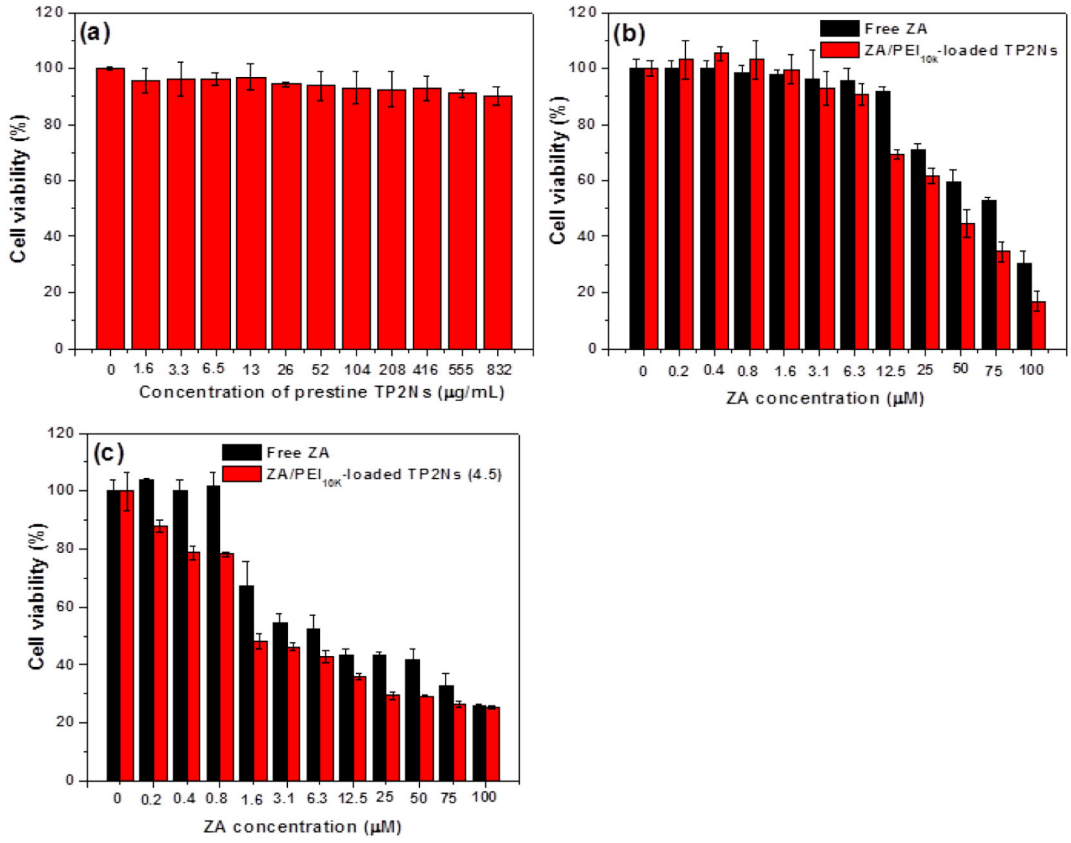

Fig. 7. Cell viability of MCF-7 cells treated with (a) ZA-free TP2Ns, (b) free ZA and ZA/PEI_{10k}-loaded TP2Ns, respectively, at 37 °C for 48 h. (c) Cell viability of TRAMP-C1 cells incubated with free ZA and ZA/PEI_{10k}-loaded TP2Ns, respectively, at 37 °C for 48 h.

Acknowledgements

This work is supported by the Ministry of Science and Technology, Taiwan (MOST 107-2622-E-005-008-CC3, MOST 108-2221-E-005-024-MY2 and MOST 108-2731-M-005-001).

Appendix A. Supplementary data

Supplementary data to this article can be found online at https://doi.org/10.1016/j.msec.2020.111277.

References

[1] K.M. Au, A. Satterlee, Y. Min, X. Tian, Y Kim .S., J.M. Caster, L. Zhang, T. Zhang, L. Huang, A.Z. Wang, Folate-targeted pH-responsive calcium zoledronate nanoscale metalorganic frameworks: turning a bone antiresorptive agent into an anticancer therapeutic, Biomaterials 82 (2016) 178–193.

[2] X. Li, Y.W. Naguib, Z. Cui, In vivo distribution of zoledronic acid in a bisphosphonate-metal complex-based nanoparticle formulation synthesized by a reverse microemulsion method, Int. J. Pharm. 526 (2017) 69–76.

[3] J.R. Berenson, L.S. Rosen, A. Howell, L. Porter, R.E. Coleman, W. Morley, et al., Zoledronic acid reduces skeletal-related events in patients with osteolytic metastases, Cancer 91 (2001) 1191–1200.

[4] K. McKeage, G.L. Plosker, Zoledronic acid: a pharmacoeconomic review of its use in the management of bone metastases, Pharmacoeconomics 26 (2008) 251–268.

[5] H. Almubarak, A. Jones, R. Chaisuparat, M. Zhang, T.F. Meiller, M.A. Scheper, Zoledronic acid directly suppresses cell proliferation and induces apoptosis in highly tumorigenic prostate and breast cancers, J. Carcinog. 10 (2011) 2.

[6] J. Zekri, M. Mansour, S.M. Karim, The anti-tumor effects of zoledronic acid, Oncology 2 (2014) 25–35.

[7] D. Desai, J. Zhang, J. Sandholm, J. Lehtimäki, T. Grönroos, J. Tuomela, J.M. Rosenholm, Lipid bilayer-gated mesoporous silica nanocarriers for tumor-targeted delivery of zoledronic acid in vivo, Mol. Pharm. 14 (2017) 3218–3227.

[8] C. Borghese, N. Casagrande, E. Pivetta, A. Colombatti, M. Boccellino, E. Amler, N. Normanno, M. Caraglia, G.D. Rosa, D. Aldinucci, Self-assembling nanoparticles encapsulating zoledronic acid inhibit mesenchymal stromal cells differentiation, migration and secretion of proangiogenic factors and their interactions with prostate cancer cells, Oncotarget 8 (2017) 42926–42938.

[9] J. Kopecka, S. Porto, S. Lusa, E. Gazzano, G. Salzano, A. Giordano, V. Desiderio, D. Ghigo, M. Caraglia, G.D. Rosa, C. Riganti, Self-assembling nanoparticles encapsulating zoledronic acid revert multidrug resistance in cancer cells, Oncotarget 6 (2015) 31461–31478.

[10] P. Tsagozis, F. Eriksson, P. Pisa, Zoledronic acid modulates antitumoral responses of prostate cancer-tumor associated macrophages, Cancer Immunol. Immunother. 57 (2008) 1451–1459.

[11] X. Zang, X. Zhang, H. Hu, M. Qiao, X. Zhao, Y. Deng, D. Chen, Targeted delivery of zoledronate to tumor-associated macrophages for cancer immunotherapy, Mol. Pharm. 16 (2019) 2249–2258.

[12] X. Tang, C. Mo, Y. Wang, D. Wei, H. Xiao, Anti-tumour strategies aiming to target tumour-associated macrophages, Immunology 138 (2013) 93–104.

[13] M. McClung, Bisphosphonates, Arq. Bras. Endocrinol. Metab. 50 (2006) 735–744.

[14] D. Kimmel, Mechanism of action, pharmacokinetic and pharmacodynamic profile, and clinical applications of nitrogen-containing bisphosphonates, J. Dent. Res. 86 (2007) 1022–1033.

[15] H.M. Weiss, U. Pfaar, A. Schweitzer, H. Wiegand, A. Skerjanec, H. Schran, Biodistribution and plasma protein binding of zoledronic acid, Drug Metab. Dispos. 36 (2008) 2043–2049.

[16] X. Li, S.A. Valdes, R.F. Alzhrani, S. Hufnagel, S.D. Hursting, Z. Cui, Zoledronic acid-containing nanoparticles with minimum premature release show enhanced activity against extraskeletal tumor, ACS Appl. Mater. Interfaces 11 (2019) 7311–7319.

[17] M. Marra, G. Salzano, C. Leonetti, P. Tassone, M. Scarsella, S. Zappavigna, T. Calimeri, R. Franco, G. Liguori, G. Cigliana, et al., Nanotechnologies to use bisphosphonates as potent anticancer agents: the effects of zoledronic acid encapsulated into liposomes, Nanomedicine 7 (2011) 955–964.

[18] H. Shmeeda, Y. Amitay, D. Tzemach, J. Gorin, A. Gabizon, Liposome encapsulation of zoledronic acid results in major changes in tissue distribution and increase in toxicity, J. Control. Release 167 (2013) 265–275.

[19] Q. Guo, X. He, C. Li, Y. He, Y. Peng, Y. Zhang, Y. Lu, X. Chen, Y. Zhang, Q. Chen, T. Sun, C. Jiang, Dandelion-like tailorable nanoparticles for tumor microenvironment modulation, Adv. Sci. 6 (2019) 1901430.

[20] F. Benyettou, M. Alhashimi, M. O'Connor, R. Pasricha, J. Brandel, H. Traboulsi, J. Mazher, J.C. Olsen, A. Trabolsi, Sequential delivery of doxorubicin and zoledronic acid to breast cancer cells by CB[7]-modified iron oxide nanoparticles, ACS Appl. Mater. Interfaces 9 (2017) 40006–40016.

[21] J. Liu, D.Ş. Karaman, J. Zhang, J.M. Rosenholm, X. Guo, K. Cai, NIR light-activated dual-modality cancer therapy mediated by photochemical internalization of porous nanocarriers with tethered lipid bilayers, J. Mater. Chem. B 5 (2017) 8289–8298.

[22] X. Li, Y.W. Naguib, S. Valdes, S. Hufnagel, Z. Cui, Reverse microemulsion-based synthesis of (bis)phosphonate-metal materials with controllable physical properties: an example using zoledronic acid-calcium complexes, ACS Appl. Mater. Interfaces 9 (2017) 14478–14489.

[23] E. Locatelli, M. Comes Franchini, Biodegradable PLGA-b-PEG polymeric nanoparticles: synthesis, properties, and nanomedical applications as drug delivery system, J. Nanopart. Res. 14 (2012) 1316.

[24] Y. Lee, D. Chang, Fabrication, characterization, and biological evaluation of anti-HER2 indocyanine green-doxorubicin-encapsulated PEG-b-PLGA copolymeric nanoparticles for targeted photochemotherapy of breast cancer cells, Sci. Rep. 7 (2017) 46688.

[25] H. Choudhury, B. Gorain, M. Pandey, S.A. Kumbhar, R.K. Tekade, A.K. Iyer, P. Kesharwani, Recent advances in TPGS-based nanoparticles of docetaxel for improved chemotherapy, Int. J. Pharm. 529 (2017) 506–522.

[26] Y. Xing, J. Zhang, F. Chen, J. Liu, K. Cai, Mesoporous polydopamine nanoparticles with co-delivery function for overcoming multidrug resistance via synergistic chemo-photothermal therapy, Nanoscale 9 (2017) 8781–8790.

[27] W. Chen, W. Yang, P. Chen, Y. Huang, F. Li, Disulfiram copper nanoparticles prepared with a stabilized metal ion ligand complex method for treating drug-resistant prostate cancers, ACS Appl. Mater. Interfaces 10 (2018) 41118–41128.

[28] I. Insua, A. Wilkinson, F. Fernandez-Trillo, Polyion complex (PIC) particles: preparation and biomedical applications, Eur. Polym. J. 81 (2016) 198–215.

[29] Z. Chen, Z. Lv, Y. Sun, Z. Chi, G. Qing, Recent advancements in polyethyleneimine-based materials and their biomedical, biotechnology, and biomaterial applications, J. Mater. Chem. B 8 (2020) 2951–2973.

[30] B.N. Abd El-Hamid, N.K. Swarnakar, G.M. Soliman, M.A. Attia, G.M. Pauletti, High payload nanostructured lipid carriers fabricated with alendronate/polyethyleneimine ion complexes, Int. J. Pharm. 535 (2018) 148–156.

[31] S.C. Liao, C.W. Ting, W.H. Chiang, Functionalized polymeric nanogels with pH-sensitive benzoic-imine cross-linkages designed as vehicles for indocyanine green delivery, J. Colloid Interface Sci. 561 (2020) 11–22.

[32] A.E. Smith, X. Xu, S.E. Kirkland-York, D.A. Savin, C.L. McCormick, "Schizophrenic" self-assembly of block copolymers synthesized via aqueous RAFT polymerization: from micelles to vesicles, Macromolecules 43 (2010) 1210–1217.

[33] Y.F. Huang, W.H. Chiang, P.L. Tsai, C.S. Chern, H.C. Chiu, Novel hybrid vesicles co-assembled from a cationic lipid and PAAc-g-mPEG with pH-triggered transmembrane channels for controlled drug release, Chem. Commun. 47 (2011) 10978–10980.

[34] H. Wen, H. Dong, J. Liu, A. Shen, Y. Li, D. Shi, Redox-mediated dissociation of PEG-polypeptide-based micelles for on-demand release of anticancer drugs, J. Mater. Chem. B 4 (2016) 7859–7869.

[35] W.H. Jian, T.W. Yu, C.J. Chen, W.C. Huang, H.C. Chiu, W.H. Chiang, Indocyanine green-encapsulated hybrid polymeric nanomicelles for photothermal cancer therapy, Langmuir 31 (2015) 6202–6210.

[36] U. Lungwitz, M. Breunig, T. Blunk, A. Göpferich, Polyethylenimine-based non-viral gene delivery systems, Eur. J. Pharm. Biopharm. 60 (2005) 247–266.

[37] J. Wang, B. Doub, Y. Bao, Efficient targeted pDNA/siRNA delivery with folate-low-molecular-weight polyethyleneimine-modified pullulan as non-viral carrier, Mater. Sci. Eng. C 34 (2014) 98–109.

[38] E. Blanco, H. Shen, M. Ferrari, Principles of nanoparticle design for overcoming biological barriers to drug delivery, Nat. Biotechnol. 33 (2015) 941–951.

[39] H.T.M. Phan, S. Bartelt-Hunt, K.B. Rodenhausen, M. Schubert, J.C. Bartz, Investigation of bovine serum albumin (BSA) attachment onto self-assembled monolayers (SAMs) using combinatorial quartz crystal microbalance with dissipation (QCM-D) and spectroscopic ellipsometry (SE), PLoS One 10 (2015) e0141282.

[40] D.K. Khajuria, R. Razdan, D.R. Mahapatra, Development, in vitro and in vivo characterization of zoledronic acid functionalized hydroxyapatite nanoparticle based formulation for treatment of osteoporosis in animal model, Eur. J. Pharm. Sci. 66 (2015) 173–183.

[41] D. Klose, F. Siepmann, J.F. Willart, M. Descamps, J. Siepmann, Drug release from PLGA-based microparticles: effects of the "microparticle:bulk fluid" ratio, Int. J. Pharm. 383 (2010) 123–131.

[42] M.C. Fontana, K. Coradini, A.R. Pohlmann, S.S. Guterres, R.C. Beck, Nanocapsules prepared from amorphous polyesters: effect on the physicochemical characteristics, drug release, and photostability, J. Nanosci. Nanotechnol. 10 (2010) 3091–3099.

[43] H.K. Makadia, S.J. Siegel, Poly lactic-co-glycolic acid (PLGA) as biodegradable controlled drug delivery carrier, Polymers 3 (2011) 1377–1397.

[44] Y. Zhai, F. Ishizuka, M.H. Stenzel, A.M. Granville, P.B. Zetterlund, Synthesis of polydopamine capsules via SPG membrane emulsion templating: tuning of capsule size, J. Polym. Sci. Part A: Polym. Chem. 55 (2017) 365–370.

[45] H. Ejima, J.J. Richardson, F. Caruso, Phenolic film engineering for template-mediated microcapsule preparation, Polym. J. 46 (2014) 452–459.

[46] G.K. Jain, S.A. Pathan, S. Akhter, N. Ahmad, N. Jain, S. Talegaonkar, R.K. Khar, F.J. Ahmad, Mechanistic study of hydrolytic erosion and drug release behaviour of PLGA nanoparticles: influence of chitosan, Polym. Degrad. Stab. 95 (2010) 2360–2366.

[47] K.A. Curtis, D. Miller, P. Millard, S. Basu, F. Horkay, P.L. Chandran, Unusual salt and pH induced changes in polyethylenimine solutions, PLoS One 11 (2016) e0158147.

[48] M. Wojnilowicz, A. Glab, A. Bertucci, F. Caruso, F. Cavalieri, Super-resolution imaging of proton sponge-triggered rupture of endosomes and cytosolic release of small interfering RNA, ACS Nano 13 (2019) 187–202.

[49] L. Zhu, P. Li, D. Gao, J. Liu, Y. Liu, C. Sun, M. Xu, X. Chen, Z. Sheng, R. Wang, Z. Yuan, L. Cai, Y. Ma, Q. Zhao, pH-sensitive loaded retinal/indocyanine green micelles as an "all-in-one" theranostic agent for multi-modal imaging in vivo guided cellular senescence-photothermal synergistic therapy, Chem. Commun. 55 (2019) 6209–6212.

[50] P. Zhang, Q. Xu, X. Li, Y. Wang, pH-responsive polydopamine nanoparticles for photothermally promoted gene delivery, Mater. Sci. Eng. C 108 (2020) 110396.

[51] D. Zhang, L. Wei, M. Zhong, L. Xiao, H.W. Li, J. Wang, The morphology and surface charge-dependent cellular uptake efficiency of upconversion nanostructures revealed by single-particle optical microscopy, Chem. Sci. 9 (2018) 5260–5269.

[52] D. Liu, S.A. Kramer, R.C. Huxford-Phillips, S. Wang, J. Della Rocca, W. Lin, Coercing bisphosphonates to kill cancer cells with nanoscale coordination polymers, Chem. Commun. 48 (2012) 2668–2670.